ION DYNAMICS AND DISTRIBUTION AT THE QUASIPERPENDICULAR COLLISIONLESS SHOCK FRONT

M. Gedalin
Ben-Gurion University, P.O. Box 653, Beer-Sheva, 84105, Israel

Abstract. Collisionless shocks are well-known to be very efficient energizers of ions. At the first step of energization relatively low energy suprathermal ion distributions are formed in the vicinity of the quasiperpendicular collisionless shock front during ion reflection and direct transmission. These distributions are formed promptly and at the scale of the shock width mainly due to the ion interaction with the quasistationary electromagnetic structure of the front itself. Their features are intimately related to the fine structure of the shock front in the sense that they depend not only on the bulk shock parameters, such as Mach number, but also on the details of the distribution of the fields, in particular, shock width. Therefore, studies of these distributions may provide valuable information about the shock structure itself. We review the observational data collected during in situ measurements (mainly at the Earth bow shock) and compare it to the numerical simulations and theoretical developments. The developed theory of the ion dynamics in the stationary shock front relates the ion reflection and heating to the insufficient deceleration of the ions in the ramp by the cross-shock potential, as compared to the expected downstream drift velocity, required by the Rankine-Hugoniot relations. As a result, the direct flow energy it transferred into the gyration energy, leading to the gyration of the ion distribution as a whole and enhanced spread in the velocity space, that is, effective collisionless heating. Anisotropy and nongyrotropy are typical features of ion distributions at both low and high-Mach number shocks, which is confirmed by observations. Time-dependent fields, which are not considered in the stationary shock mode, are thought to provide subsequent smoothing and isotropization of the ion distributions. These processes occur at scales substantially larger than the shock width.

Keywords: Collisionless shocks, ion reflection, ion heating, ion dynamics, fine structure, nongyrotropy

To the memory of Les Woolliscroft, friend and colleague

1. Introduction

Collisionless shocks are one of the most ubiquitous phenomena in space plasmas. They are suspected to be very efficient accelerators of charged particles, in particular ions (see, e.g. Blandford and Eichler (1987) for review and references). The energy, which an ion can achieve, depends

on the scale at which it is accelerated. Highest energies are achieved within the diffusive shock acceleration at scales which are much larger than the typical shock width. It is these energies in which we are ultimately interested. Much lower (slightly suprathermal) energies are achieved during ion reflection and heating at the shock front. The significance of these low energy ion distributions is related to the fact that they are formed promptly and at small scales, so that they are intimately related to the instantaneous fine structure of the shock front. These small scale low energy processes seem to determine the basic shock parameters, like the compression ratio, which in turn determine the efficiency of much more powerful acceleration processes. Reflected ions, in particular, are believed to provide necessary dissipation in the high-Mach number supercritical shocks to maintain their quasi-stationary structure (see, e.g., Gosling and Robson, 1985). Last but not least, it is highly probable that these processes provide the first seed population of suprathermal particles to be injected afterwards into the diffusive mechanism of acceleration.

The ion energization is strong at all shocks, both quasiparallel (in which the angle between the shock normal and upstream magnetic field $\theta < 45^\circ$) and quasiperpendicular (in which $\theta > 45^\circ$). However, the relation of this energization to the shock structure may be different in the two cases, since quasiparallel shocks exhibit very turbulent non-stationary magnetic field profiles (Quest, 1988; Scholer and Fujimoto, 1993; Wilkinson *et al.*, 1993), while most quasiperpendicular shocks look quite stable and almost stationary (Kennel *et al.*, 1985; Greenstadt, 1985). Accordingly, the ion energization at quasiparallel shocks is usually attributed to the interaction with large amplitude waves and turbulence (Leroy *et al.*, 1982; Quest, 1988; Scholer and Fujimoto, 1993; Wilkinson *et al.*, 1993), while the energization at quasiperpendicular shocks is believed to be mainly due to the interaction with the quasistationary electromagnetic structure of the shock front (Sckopke *et al.*, 1983; Forslund *et al.*, 1984; Burgess *et al.*, 1989). In the present paper we consider only the ion reflection and heating at quasiperpendicular shocks.

Magnetic field profiles of collisionless shocks are rather complicated, especially at high-Mach number shocks, as shown in Figure 1a. This complicated profile is usually averaged to the well-structured quasi-stationary profile (Figure 1b), which consists of several distinct regions (Kennel *et al.*, 1985; Scudder *et al.*, 1986a): (1) extended foot where the magnetic field gradually increases, (2) the most narrow part of the front - ramp - where the main magnetic field jump occurs, and (3) overshoot and possibly large amplitude downstream oscillations. As we shall see below the reflection and heating processes occur in the shock front

region which covers the foot, ramp, and overshoot (the last only partly). It is important that the width of this energization region is smaller than the ion convective gyroradius V_u/Ω_u (where V_u is the plasma upstream velocity and $\Omega_u = eB_u/m_i$ is the upstream ion gyrofrequency), which means that the ion motion is strongly nonadiabatic.

The magnetic profile of a low-Mach number shock (as shown in Figure 2) is less complicated and consists mainly of the ramp (Russell *et al.*, 1982b; Mellott and Greenstadt, 1984; Farris *et al.*, 1993) and probably weak overshoot (Mellott and Livesey, 1987), the width of which is also substantially less than the ion convective gyroradius, and ion crosses this region in about 0.1 of its gyroperiod. Thus, in both high-Mach number and low-Mach number shocks the ion motion is substantially nonadiabatic, so that the magnetic moment is not conserved and magnetic compression does not work.

As can be seen from Figures 1 and 2, the shock profiles are highly fluctuating (both in space in time), especially in the case of the high-Mach number shock. These varying fields do affect the ion motion although their influence is believed to be weak relative to the role of the stationary fields. The distribution of the last may be more complex than is shown in Figures 1b and 2b, for example, a phasestanding precursor is argued to be present (Galeev *et al.*, 1988) just ahead of the ramp, and is indeed observed in a number of cases. Yet we stick in the present paper to the "standard" model of the shock front, corresponding to Figures 1b and 2b, given the lack of a better theory.

In the present paper we review the observational data collected during in situ measurements of ion distributions mainly at the terrestrial bow shock, and confront them against theoretical views within the framework of the stationary shock front model. The objective is to achieve a quantitative (if possible) description of the ion dynamics in the structured shock front and determine to what extent the observed features of the ion distributions in the shock vicinity can be understood within the idea of the ion interaction with the stationary electromagnetic fields.

2. Observations

Much data on ion heating and reflection has been collected at the terrestrial bow shock during ISEE and AMPTE missions.

2.1. ISEE Observations: High-Mach Number Shocks

A typical sequence of the ion distributions at the high-Mach number supercritical shock front is shown in Figure 3. These measurements has been done by ISEE-1 at the famous ''typical" shock crossing on November 7, 1977 (Paschmann *et al.*, 1982; Sckopke *et al.*, 1983), described in detail by Scudder *et al.* (1986a). The parameters of this shock are as follows: the Mach number $M = 7.7$, the angle between the shock normal and upstream magnetic field $\theta = 76^\circ$, the ion kinetic-to-magnetic pressure ratio $\beta_i = 0.8$, and the electron kinetic-to-magnetic pressure ratio $\beta_e = 1.6$. In the two-dimensional plots the point indicates the direction of the magnetic field out of the plane, which means that the shown distributions are approximately cuts perpendicular to the magnetic field. The small plot in the upper left corner of each distribution plot shows the accompanying 3 s average magnetic field profile and the position of the spacecraft during the measurement of the corresponding distribution.

Ahead of the foot in the upstream region (at 22:50:55) the ion distribution consists only of the incident ion beam, but when the spacecraft enters the foot (22:51:01), at the very upstream edge of it, an addition of the reflected ion beam immediately appears. The formation of this reflected ion beam has been first explained in the simplest ion specular reflection model (Woods, 1969; Woods, 1971), which assumes that some ions are reflected at the ramp by the electrostatic barrier (Woods, 1971; Leroy, 1983; Sckopke *et al.*, 1983; Schwartz *et al.*, 1983; Sckopke *et al.*, 1990; Fuselier and Schmidt, 1994) in such a way that their normal velocity changes its sign while the tangential velocity remains unchanged. These reflected ions form an ion semi-ring just ahead of the ramp, and the corresponding ion ring current is responsible for the gradual increase of the magnetic field and foot formation. Ater having been accelerated by the upstream motional electric field, these ions re-enter the ramp, cross it, and form the downstream distribution of reflected ions. The reflected ion distribution is predicted to have a form of two distinct gyrophase-bunched beams in the foot, while the downstream distribution consists of several beams, depending on the shock geometry (Sckopke *et al.*, 1983) (see Figure 4).

Actual reflected ion distribution differs from what is predicted. In particular, the reflected ion ''beam" in the foot (22:51:13-22:51:25) is much more diffuse, than could be expected from the specular reflection model, and is more dispersed than the incident ion beam itself. Realizing that the reflection is nonspecular, Sckopke *et al.* (1983) proposed as a next approximation a phenomenological model in which some ions are specularly reflected while others are almost isotropically scattered

off the ramp. This model explains the diffuse shape of the reflected ion beam and predicts almost the same foot length as the specular reflection model, which gives $L_f = 0.68(V_u/\Omega_u)$ in the perpendicular case (Woods, 1971) and larger values for oblique shocks (Gosling and Thomsen, 1985). This prediction is consistent with observations only within 100% error (Livesey *et al.*, 1984; Newbury and Russell, 1996) and should be considered as an order of magnitude estimate, when using it for the shock scale determination using single-spacecraft measurements (Newbury and Russell, 1996; Gedalin, 1996a,d).

Within the ramp (approximately at 22:51:37, due to the averaging the ramp looks wider than it is in reality, according to the high resolution data (Scudder *et al.*, 1986a)) the ion distribution consists of directly transmitted ions (those which are not reflected at all), ions which are being reflected, and those ions which have been reflected and came back to the ramp to cross it again and form the downstream distribution of the reflected ions. The downstream distribution consists of the low energetic dense core of the directly transmitted ions and high-energy low-density gyrophase-bunched component of the reflected ions. Starting from the upstream edge of the foot the ion distribution is highly non-gyrotropic even well beyond the ramp. It becomes more or less gyrotropic (although not completely) only well in the downstream region.

The contribution of the reflected ions to the overall ion distribution function is shown in Figure 5. The first profile of the distribution function corresponds to the spacecraft position just behind the ramp. The dense low energy core and low-density high-energy shoulder of reflected ions are seen quite clearly. The shoulder persists well into downstream (for more than an hour after the last distribution in Figure 3), and the ion distribution is far from being Maxwellian (shown by the dashed line). The reflected ion contribution in the ion heating, understood as the spread in the velocity space, is very substantial. Actually, in this case almost all ion heating is due to the reflected ions.

2.2. ISEE Observations: Low-Mach Number Shocks

It is relatively easy to measure and identify different components of the ion distribution (in particular, reflected ions) at high-Mach number supercritical shocks where the fraction of reflected ions can be as large as 40%. At low-Mach number shocks the reflected ion fraction (if any) constitutes only several percents of the total ion density, and the limitations of the existing devices and low density of the solar wind plasma may significantly affect the results of measurements and their interpretation.

An example of a ion distribution at a low-Mach number shock is shown in Figure 6 in the same format as in Figure 3. In this case the shock parameters were as follows: $M = 2.6$, $\theta = 75°$, $\beta_i = 0.1$, and $\beta_e = 0.3$. One could expect that the number of reflected ions would be insufficient to produce any substantial current and form a foot. Indeed, there is no noticeable foot, and the ion distribution at the very upstream edge of the ramp is the incident ion distribution. However, just behind the ramp, at the very downstream edge of it, the reflected ion component can be seen. The density of these reflected ions is very small ($< 3\%$ from the total ion density) but the energy is high and they are situated on a typical circle in the velocity space with the radius of $\sim 2V_u$. Despite the small number of reflected ions their contribution to the ion heating is significant. The rest of the features of the ion distribution are quite similar to those shown in Figure 3, and it remains non-gyrotropic even well beyond the ramp in the downstream region.

A comprehensive analysis of ion heating at low-Mach number shocks (subcritical, marginally critical, and weakly supercritical), based on ISEE measurements, has been carried out by Thomsen *et al.* (1985). Figure 7 shows the (typical) ion distribution measurements at the very low-Mach number $M = 2.1$, low $\beta_i = 0.03$, $\beta_e = 0.11$, quasiperpendicular $\theta = 62°$ shock. In this case the magnetic field was in the measurement plane and the two-dimensional plots show effectively the $(v_\parallel, v_\perp)$ cut. The spatial resolution allowed to obtain several distributions within the ramp. It is seen that the ion energization and heating begins within the ramp, and just behind the ramp the ions are already almost completely heated and the distribution does not change much afterwards (except gradual smoothing). The perpendicular heating greatly exceeds the heating in the direction parallel to the magnetic field. The distribution is clearly non-gyrotropic, since it is shifted relative to the downstream drift velocity. No reflected ions were observed in this series of measurements.

2.3. AMPTE-IRM Observations: Low-Mach Number Shocks

Later measurements at low-Mach number shocks with similar parameters, made by AMPTE-IRM (Sckopke *et al.*, 1990), did not confirm completely the results of ISEE. One of the reasons can be the difference of the measurement technique in the two experiments. The cited ISEE 1 and 2 measurements were made mostly with the joint Los Alamos/Max-Plank-Insitut Garching fast plasma experiment (FPE). The FPE detector has a shape of a fan (few degrees wide in azimuth) with an opening angle of 110° (±55° in elevation angle above and below

the spacecraft equatorial plane). The detector covers the energy range from 50 eV to 20 keV per charge in 16 contiguous energy bins (corresponding to the relative width of $\Delta v/v \approx 18\%$) and provides 16 azimuth angle measurements during one satellite rotation (3 s). This mode of measurement allows to obtain only two-dimensional distributions and involves significant averaging over energies, pitch-angles (in the best case when ions are gyrotropic and the symmetry axis coincides with the spacecraft rotation axis, otherwise the averaging over the fan opening angle is even less clear), and extensive temporal (spatial in the shock frame) averaging. In this mode of measurements the chances to loose low-density spatially-dependent strongly gyrophase-bunched ion beams might be high.

The plasma instrument of AMPTE/IRM (Paschmann *et al.*, 1985) allows measurements of three-dimensional ion distribution functions once every spacecraft rotation, that is, in 4.3 s. The whole 4π solid angle is covered in 128 channels spaced 22.5° in azimuth with an intrinsic azimuth acceptance of $\sim 6°$. The energy range from 20 eV to 40 keV per charge is covered in 30 logarithmically spaced energy channels, which corresponds to the relative width of $\Delta E/E = 0.29$. In comparison with the ISEE mode of measurements, the AMPTE/IRM mode provides almost full three-dimensional distribution free from the angular averaging. Averaging over energies is weaker, while temporal/spatial averaging is a little stronger.

An example of the ion distribution measure by AMPTE/IRM at a low-Mach number $M = 2.5$, low $\beta_i \approx 0.05$, nearly perpendicular $\theta \sim 90°$ shock is shown in Figure 8. Three two-dimensional cuts of the complete three-dimensional function are presented. Of the most interest are the second cut, corresponding to the $(v_\parallel, v_\perp)$ plane, and the third cut, which is perpendicular to the magnetic field. The upper panel corresponds to the distribution measured just behind the ramp, while the lower panel corresponds to the spacecraft position well in the magnetosheath and is apparently strongly influenced by the plasma and magnetic field features (in particular turbulent fields) in this region. The upper panel reveals features similar to what has been observed by ISEE (strong anisotropy with preferred heating perpendicular to the magnetic field and non-gyrotropy). However, in this case there is also a low density reflected ion component, which is seen as an (almost complete) high energy circle at the third plot. These ions constitute not more than 5% of the total density but contribute almost 40% of the downstream ion pressure. Similar results have been obtained at other low-Mach number shocks. Even when the reflected ion fraction was as small as $1 - 2\%$ their contribution into the downstream ion pressure was noticeable. In order to account for this apparent contradiction with

the earlier results of Thomsen *et al.* (1985) it was suggested (Sckopke *et al.*, 1990) that presence or absence of reflected ions does not depend only on the shock Mach number and/or beta, but also on other (may be unknown so far) parameters.

2.4. Observations: Summary

The existing observations show that ions are efficiently energized at both low and high-Mach number shocks. The efficiency increases quickly with the increase of the Mach number, which is related to the rapid increase of the reflected ion fraction. In the same time the reflection process in not a simple specular reflection and does not depend only on the Mach number. The ion distributions are typically substantially nongyrotropic, and gyrotropize only well beyond the ramp.

3. Numerical Simulations

Numerical analysis of the ion motion in the shock front can be carried out using test particle technique (Gedalin, 1996a) or combining analytical developments with some auxiliary quasi-self-consistent numerical calculations (Leroy, 1983). In both cases it is not a true simulation since dynamical feedback of the ion distribution on the shock front structure and self-consistency is not maintained. Therefore, these methods should be regarded as a part of the theoretical treatment. True numerical simulations of collisionless shocks are being done within hybrid or full-particle approaches (Goodrich, 1985).

3.1. Hybrid Simulations

Hybrid numerical simulations treat the field-ion coupling self-consistently but regard light electrons as a massless fluid. As a result the typical electron spatial scales, such as electron inertial length c/ω_{pe} and electron gyroradius v_{Te}/Ω_e are lost (here $\omega_{pe} = (ne^2/\varepsilon_0 m_e)^{1/2}$ is the electron plasma frequency, $\Omega_e = eB_u/m_e$ is the electron gyrofrequency, and $v_{Te} = (k_B T/m_e)^{1/2}$ is the electron thermal velocity). The lengths of the foot and overshoot are determined by ion dynamics and are of the order of the typical ion length (in this case it is the ion convective gyroradius V_u/Ω_i). It is not, however, the case for the shock ramp, the width of which can be substantially smaller than the ion inertial length c/ω_{pi} and as small as $\sim 0.1(c/\omega_{pi})$ (Scudder *et al.*, 1986b; Newbury and Russell, 1996). Theory predicts that the ramp of a nearly perpendicular shocks can be as small as c/ω_{pe} (see, for example, Galeev *et al.* (1988) and

references therein). Hence, hybrid simulations may provide incorrect scaling of the shock front, in particular, in the region where the ion energization occurs. As we shall see below details of the electromagnetic field distribution in the shocks front, in particular, ramp width, are significant for quantitative description of ion dynamics. Nevertheless, qualitative description of the ion motion in the shock front within the hybrid numerical simulations is quite reliable.

Numerous simulations of quasi-perpendicular shocks (see Goodrich, 1985 for review) have elucidated the role of ion reflection at high-Mach number shocks and relation of the reflected and directly transmitted ions to the shock profile and stability, although details of the ion reflection (within hybrid simulations) were comprehensively studied only relatively recently (Burgess *et al.*, 1989). Burgess *et al.* succeeded to separate reflected and directly transmitted ions to show that the reflection condition is not related directly to the ion velocity along the shock normal x (as could be expected in the case of the electrostatic braking), but is controlled by the initial ion velocity component v_y along the shock normal, which emphasizes the role of the magnetic deflection (Leroy *et al.*, 1982). These ions came from the wing of the incident ion distribution function. They were found to be turned around (reflected) in the vicinity of the overshoot (or near the electric potential maximum), well beyond the ramp, thus indicating behavior different from predicted by the specular reflection model. The directly transmitted ions formed a relatively cold beam which gyrated as a whole in the downstream region behind the ramp. The contribution of the reflected ions into the downstream ion heating substantially exceeded the contribution of the directly transmitted ions, which provided most of the downstream ion density.

For obvious reasons much more attention has been paid to the ion reflection than to the directly transmitted ion population, which dominates in the low-Mach number shocks. Few hybrid simulations (Lee *et al.*, 1987; Wilkinson, 1991) were devoted specially to the ion dynamics and heating at the low-Mach number shock front. The main conclusion of these analyses is that the contribution of the reflected ions into the ion heating increases very rapidly with the increase of the Mach number (and shock strength, respectively). Wilkinson (1991) showed that the downstream ion pressure is strongly spatially variable and anisotropic even in the case of the very low-Mach number shocks where there are almost no reflected ions. This behavior of ions was attributed by Wilkinson to "kinetic effects".

3.2. Full Particle Simulations

Full particle simulations treat both species (ions and electrons) as massive particles and could be very effective in the determination of the shock-particle interaction. In practice, however, computer requirements (reasonable computing time) greatly restrict the number of particles which can be analyzed, the mass ratio, and the frequency ratio ω_{pe}/Ω_e. Thus, Forslund *et al.* (1984) use the mass ratio $m_i/m_e = 100$ and $\omega_{pe}/\Omega_e = 20$. Although this mass ratio is probably sufficient to separate the ion and electron lengths c/ω_{pi} and c/ω_{pe} by an order of magnitude, the second parameter shows that $v_A/c = 1/200$, which is by two orders of magnitude higher than in reality. As a result, the corresponding electric field of a magnetosonic wave, for example, is by two orders of magnitude stronger than it is at the Earths bow shock. The simulations have shown a rather high level of turbulence at the shock front, which resulted in the reduction of ion reflection. There is no much difference between the hybrid-code and particle-code determined ion phase spaces which clearly show substantial role of reflected ions.

It is difficult to make unambiguous conclusions about the ion dynamics and ion distribution formation at the shock front from self-consistent numerical simulations. First, tracing ion trajectories is a complicated task and is not usually performed. Second, stationary and time-varying electromagnetic fields can not be separated in such analysis and in most cases their relative importance remains unclear. For instance, it is often inconsistently assumed that the foot length is determined by the ions that are reflected in the stationary shock front, while their diffuse distribution is due to turbulent scattering. Additional problems may be related to the reduced dimensionality of the numerical simulations (three-dimensional simulations are extremely computer time consuming) (Jokipii *et al.*, 1993; Giacalone *et al.*, 1994).

3.3. Numerical Simulations: Summary

Numerous simulations allowed to reproduce numerically many of the features of the observed ion distributions. Yet the description is not complete, because of difficulties, related to reduced dimensionality of the simulations, low mass-ratio, and other computing problems. The parameters used in the numerical simulations, are known (observationally) only approximately, so that one has to assume low sensitivity of the results to the exact parameters, which might be not the case. While it is believed that the simulations support the point of view that the ion interaction with the stationary fields dominates, precise physical interpretation is difficult since it is not possible to separate stationary and time-dependent fields in self-consistent modeling.

4. Theory

Existing theoretical models of the ion dynamics in the shock front assume that the electric and magnetic fields in the shock depend only on the coordinate along the shock normal and are time independent. Beginning with the simplest specular reflection approach these models developed into the semi-quantitative description of the complicated ion motion in a structured finite width shock.

4.1. Specular and Nearly-Specular Reflection

First theoretical analysis of the ion motion and reflection at the shock front has been done within the step-like model of the perpendicular shock, with the zero-width magnetic field and potential jump, and constant upstream and downstream fields (Woods, 1969,1971). It was assumed that the potential jump somehow picks up some ions from the incident (almost cold) ion beam and reflects them specularly, that is, in such a way, that the normal component of the ion velocity changes its sign at the ramp, while the tangential component remains unchanged. This approach allows complete analytical consideration, which shows that the reflected ion (initially having the velocity $(V_u, 0, 0)$, where x is along the shock normal, and z is along the magnetic field), turns around at $d \approx -0.68(V_u/\Omega_u)$. Since the initial ion velocity dispersion $v_T/V_u = \sqrt{\beta_i/2}/M$ is small in high-Mach number shocks with $\beta_i \lesssim 1$, the above length provides us with the measure of the foot width. Similar analysis in the oblique ($\theta \neq 90^\circ$) shock front (Gosling and Thomsen, 1985) resulted in the following expression

$$d = -\frac{V_u}{\Omega_u}[\psi(2\cos^2\theta - 1) + 2\sin^2\theta \sin\psi], \tag{1}$$

$$\cos\psi = \frac{1 - 2\cos^2\theta}{2\sin^2\theta}, \tag{2}$$

which has been widely used for the determination of the shock velocity from single-spacecraft measurements. Large deviations (Livesey *et al.*, 1984; Gosling and Thomsen, 1985) of the independently determined foot lengths from those predicted by (1) and (2) show that the reflection process is more complicated than it is described by the simple specular reflection model. It it worthwhile to mention that such specular reflection requires that the cross-shock potential $\Delta\phi = m_i V_u^2/2e$, which is too high (Goodrich, 1985).

The following step was done by introducing into consideration the shock structure, namely, the gradual magnetic field increase in the foot. Leroy *et al.* (1982) showed that the incident ions, entering the foot,

are significantly deflected in the direction perpendicular to the shock normal and magnetic field. He concluded that this deflection adds to the electrostatic potential to provide a higher effective potential jump. The underlying idea was that this effective potential would be able to specularly reflect ions at the ramp. Self-consistent distribution of the ions and magnetic field in the foot was obtained numerically using ion hydrodynamics and matching distributions at the ramp. Ions being reflected were not allowed to cross the ramp and their velocities just before and after reflection were related as in the specular reflection model: $v_x \rightarrow -v_x$, $v_y \rightarrow v_y$. It was shown that such partially self-consistent configurations exist, when the reflected ion fraction (which was a free parameter) is not too high. The obvious disadvantage of the approach was extraordinarily high magnetic field in the foot (up to three times greater than the upstream magnetic field) starting directly from the upstream edge of it, which is not confirmed by observations. Yet the required cross-shock potential remained substantially higher than was found observationally (Scudder *et al.*, 1986b) and numerically (Goodrich, 1985; Burgess *et al.*, 1989). Further analysis of the parametric dependence of the ion reflection (Wilkinson and Schwartz, 1990) have also shown that the required cross-shock potential is too high. In particular, it was shown that at $M > 5$ the cross-shock potential $\Delta\phi = m_i V_u^2/2e$, which is not consistent with the shock hydrodynamics.

4.2. Nonspecular Reflection at High-Mach number shocks

It is rather natural to proceed further and extend the principles of the analysis of Leroy *et al.* (1982) onto the whole shock front, including ramp and overshoot (Gedalin, 1996a). To describe the analysis let us assume that the shock normal is along x and the main magnetic field is along z. We adopt the usual assumption of the one-dimensional stationary shock model (Woods, 1971; Schwartz *et al.*, 1983; Wilkinson and Schwartz, 1990) that the electromagnetic field depend only on x. Then the fields take the following form (in the normal incidence frame where the upstream fluid velocity is along the shock normal): $\mathbf{B} = (B_x, B_y, B_z)$, where $B_x = \text{const}$, and B_y is substantial only within the shock transition layer, $\mathbf{E} = (E_x, E_y, 0)$, where the cross-shock electrostatic field $E_x = -d\phi/dx$, while $E_y = V_u B_u = \text{const}$ is the motional electric field, which makes the incident ion to drift along the shock normal. The ion equations of motion look as follows:

$$\dot{v}_x = \frac{e}{m_i} E_x + \frac{e}{m_i}(v_y B_z - v_z B_y), \tag{3}$$

$$\dot{v}_y = \frac{e}{m_i} E_y + \frac{e}{m_i}(v_z B_x - v_x B_z), \tag{4}$$

$$\dot{v}_z = \frac{e}{m_i}(v_x B_y - v_y B_x), . \tag{5}$$

Since the field depend only on x let us substitute $d/dt = v_x(d/dx)$. Then the above equations can be rewritten in the following equivalent form:

$$v_x^2 = v_x^2(0) - \frac{2e\phi}{m_i} + 2\int_0^x dx(v_y\Omega_z - v_z\Omega_x), \tag{6}$$

$$v_y = v_y(0) + \int_0^x dx(\Omega_u \sin\theta \frac{V_u}{v_x} + \Omega_x \frac{v_z}{v_x} - \Omega_z), \tag{7}$$

$$v_z = v_z(0) + \int_0^x dx(\Omega_y - \Omega_x \frac{v_y}{v_x}), \tag{8}$$

where $\Omega_{x,y,z} = eB_{x,y,z}/m_i$, and for simplicity the initial conditions are taken as $\mathbf{v} = \mathbf{v}(0)$, $x = 0$, and $\phi = 0$ at $t = 0$. In our present context $x = 0$ is the beginning of the foot, and $\mathbf{B} = (B_u \cos\theta, 0, B_u \sin\theta)$ when $x < 0$. Now it is easy to roughly estimate the velocity deflection at distance L as $\Delta v_y/V_u \lesssim \Delta\Omega_z L/V_u$ and $\Delta v_z/V_u \lesssim v_T\Omega_u \cos\theta L/V_u$. The length of the foot (which is the largest scale in our case) is $\sim 0.5(V_u/\Omega_u)$, and $\Delta\Omega_z/\Omega_u \sim 0.5$, so that the deflection velocity remains small and perturbation approach is appropriate.

For the semi-quantitative description it is convenient to use the simplified model in which there is no potential drop across the foot (length L_f), the ramp length is negligible, and the overshoot is regarded as a constant $B_z = B_o$ region. Then it is easy to find that an ion with the initial velocity (v_x, v_y, v_z) will have the velocities (for simplicity we consider the perpendicular case only)

$$u_y \approx v_y + \frac{V_u\Omega_u L_f}{v_x} - A, \tag{9}$$

$$u_x^2 = v_x^2 - \frac{e\phi}{m_i} + \frac{2eV_u}{m_i v_x}A - \frac{e}{m_i}A^2, \tag{10}$$

$$A = \int_0^{L_f} \Omega_z dx, \tag{11}$$

just when it enters the overshoot. The subsequent behavior of the ion depends on the relation between u_x and expected drift velocity $v_D = V_u B_u/B_o$ in the overshoot, and also on the effective gyrophase of the ion $\psi = \arctan(u_y/(u_x - v_D))$. Once the deceleration by the cross-shock potential is insufficient to reduce the initial ion velocity and match it the expected downstream drift velocity, the ion begins to gyrate and is drifting towards downstream. Those ions which gyrate and are transmitted downstream constitute the downstream distribution of directly transmitted ions. This distribution gyrates as a whole and

periodically broadens and compresses, so that the corresponding ion pressure is a spatially periodic function (Gedalin, 1996c).

It appears that some ions from the wings of the initial distribution may have sufficiently high gyration velocities and proper gyrophases to come back to the ramp, cross it again and be found in the foot as the reflected ions. The reflection condition depends on the details of the magnetic and electric field distribution in the shock front (Gedalin, 1996a). In the above simplified model the process depends on the foot length, increase of the magnetic field across the foot, cross-shock potential, and magnetic compression ratio at the overshoot against upstream. The last parameter is the most important, since it controls the drift velocity in the overshoot and greatly affects the gyration velocity and gyrophase. The number of reflected ions, obviously, depends also on the relative ion thermal velocity v_T/V_u.

The above semi-qualitative picture is better illustrated by the following figures, obtained by direct numerical analysis of the ion trajectories in a model shock front, similar to the profile shown in Figure 1b (see details in Gedalin, 1996a). The principles of choosing the model profile are described by Gedalin *et al.* (1995) and Gedalin (1996a), and are based on the observational profiles of the magnetic field (Scudder *et al.*, 1986a,b), theoretical and observational analysis of the noncoplanar magnetic field component (Jones and Ellison, 1987; Gosling *et al.*, 1988; Jones and Ellison, 1991; Gedalin, 1996b), and available information about the cross-shock electric field (Goodrich and Scudder, 1984; Scudder *et al.*, 1986b; Wygant *et al.*, 1987). Figure 9 shows the trajectories of 25 ions in the structured front of the high-Mach number supercritical shock ($M = 6$, $B_z/B_u(\max) = 5$, $B_{zd}/B_{zu} = 3$, ramp width $\approx 0.3(c/\omega_{pi}$, $\theta = 75^\circ$, $\beta_i = 0.8)$. In our case it represents also (roughly) the ion velocity space at different spatial positions. The aforementioned features (separation between directly transmitted and reflected ions, gyration of the distributions as a whole, periodic broadening) are clearly seen. It is worthwhile to mention that the ion pressure becomes non-gyrotropic (non-diagonal in the shock coordinates) both in the foot and downstream (Gedalin and Zilbersher, 1995; Gedalin, 1996c) (see Gurgiolo *et al.* (1981); Li *et al.* (1995) for observational evidence of the ion non-gyrotropy and Brinca *et al.* (1993) for stability issues). It has been shown that the non-diagonal component of the ion pressure is closely related to the noncoplanar component of the magnetic field and cross-shock potential distribution over the extended region of the shock (Gedalin and Zilbersher, 1995; Gedalin, 1996b). The reflected ion distribution in the foot is rather diffuse, in contrast with the predictions of the specular reflection model and in agreement with observations. This is because of the long paths of the reflected ion

trajectories which pass well beyond the ramp: two initially close ion trajectories have enough time to diverge to a substantial distance in the velocity space. It is worthwhile to mention also that the foot length, which is determined by the turnaround distance of the reflected ion, is significantly smaller than it in the specular reflection model. This fact may have serious implications for the method of the shock width determination according to the foot crossing time in the single-spacecraft measurements.

Figure 10 shows the part of the incident distribution function which is reflected. The incident distribution is taken Maxwellian at the upstream edge of the foot, where it is yet undisturbed. It is clearly seen that the reflection is controlled by higher $(v_x - V_u)^2 + v_y^2$ and negative v_y (see also Burgess *et al.* (1989)). It is clear also that the not only the number of reflected ions, but also the turnaround distance and the foot length should depend on β_i, generally (cf. Figure 9). Thus, the simple expression for the foot length by Gosling and Thomsen (1985), including only the Mach number and the angle between the shock normal and upstream magnetic field, may be imprecise and provide only an order of magnitude estimate.

The downstream distribution is also diffuse, in agreement with observations. Because of the assumed constancy of the downstream magnetic field the downstream pressure is spatially periodic function of x (in the perpendicular case). In reality this periodicity should be smeared out by the irect gyrophase mixing (in the oblique geometry), effective gyrophase scattering on the inhomogeneous magnetic field, and interaction with time-dependent turbulent fields (see, for example, McKean *et al.* (1995)).

4.3. Low-Mach Number Shocks: Directly Transmitted Ions

The behavior of the directly transmitted ions should be qualitatively the same in both high-Mach number shocks and low-Mach number shocks (where it is the main component of the downstream ion distribution). Quantitative differences arise because of the lower magnetic compression ratio, higher relative cross-shock potential, typically higher $v_T/V_u \propto 1/M$, and larger ramp width in the low-Mach number shocks. Figure 11 shows the trajectories of 25 ions in the model profile of the perpendicular low-Mach number shock (as is shown in Figure 2b), with the parameters $M = 2.5$, $B_d/B_u = 2.5$, $\beta_i = 0.1$, $\theta = 76^\circ$, and ramp width of c/ω_{pi}. It is seen that the distribution strongly gyrates as a whole and several ions have rather high gyration velocities. Periodic broadening of the distribution is also clearly seen, it is responsible for the spatially periodic oscillations of the ion pressure, found earlier in

hybrid simulations (Wilkinson, 1991). The maximum downstream ion temperature exceeds the adiabatic value (Gedalin, 1996c).

The case of the low β_i can be analyzed analytically (Gedalin, 1996c) (see also Balikhin and Wilkinson (1996)). In the simplified approximation of the perpendicular shock with a zero width ramp the density n, velocity V_i, and pressure p_{ij} at the downstream edge of the ramp take the following form:

$$n = n_u(1-\varphi)^{-1/2}, \tag{12}$$

$$V_x = V_u(1-\varphi)^{1/2}, \quad V_y = 0, \tag{13}$$

$$T_{xx} = p_{xx}/nk_B = T_u(1-\varphi)^{-1}, \tag{14}$$

$$T_{yy} = p_{yy}/nk_B = T_u, \tag{15}$$

$$T_{xy} = p_{xy}/nk_B = T_u(1-\varphi)^{-1/2}, \tag{16}$$

where subscript u denotes upstream and $\varphi = 2e\phi/mV_u^2$. The heating at the ramp

$$T_r/T_u = (T_{xx}+T_{yy})/2T_u = (1+(1-\varphi)^{-1})/2, \tag{17}$$

and estimating $\varphi = 2((B_d/B_u)-1)/M^2$ (Gedalin and Zilbersher, 1995), one finds that for low Mach number shocks with $M = 2-2.5$, $B_d/B_u = 2-2.5$, the heating at the ramp $T_d/T_u \approx 1.5$.

Further downstream the ion density, velocity, and pressure can be expressed in the parametric form and are periodic on x with the maximum heating of about (Gedalin, 1996c)

$$\frac{T_{max}}{T_u} = \min \quad [\frac{R^2(1-\varphi)}{2(1-R(1-\varphi)^{1/2})^2}, \frac{M^2}{\beta_i}(2\lambda-(1-\varphi)^{1/2})^2], \tag{18}$$

where $R = 1/\lambda = B_d/B_u$.

The above analytical calculations do not allow to catch special and marginal cases, for example, single reflected ions if any. Figure 12 shows the ion distribution obtained numerically for the case of a perpendicular very low-Mach number ($M = 2$, B_d/B_u) shock. Traces of reflected ions are clearly seen in the second plot, which corresponds to the upstream region near the ramp. These reflected ions appear in contradiction to all expectations. This finding supports the idea that ion reflection is very sensitive to the shock structure and depends on more than one parameter (Mach number) (Sckopke *et al.*, 1990; Gedalin, 1996a). It is interesting to mention that these reflected ions disappeared when the Mach number and B_d/B_u were increased.

The typical downstream ion distribution for the case in Figure 10 is shown in Figure 13. It possesses all above described features (anisotropy and non-gyrotropy) and resembles the observed distribution (Sckopke *et al.*, 1990).

4.4. Theory: Summary

Theoretical analysis of the stationary shock model shows that the basic features of the ion energization in the shock front do find proper description within the model. Energy transfer from direct flow to gyrational degrees of freedom with subsequent spread in the velocity space is satisfactory described. Dependence of ion reflection upon the shock fine structure also finds its explanation. At the same time, better smoothness of the observed distributions should be probably attributed to the interaction with waves of other features, which are not included in the model.

5. Conclusions

Numerous observations, numerical simulations, and theoretical developments show that anisotropy and non-gyrotropy are typical features of energized ion distributions (downstream and in the foot) both in low and high-Mach number shocks. It is clear that the free energy, necessary for the ion reflection and heating, comes from the directed incident ion energy and is released during the ion deceleration at the ramp. Insufficient deceleration (relative to the expected drift velocity required by the Rankine-Hugoniot relations) results in the transformation of the directed flow energy into the gyration energy and leads to the effective collisionless ion heating. Observed patterns of the ion heating are formed also due to the initial non-gyrotropy of the energized ions and (quasi)periodic behavior of their distribution in space. This energization process is intimately related to the fine structure of the shock front in the sense that the features of the ion distributions depend not only on the global shock parameters (like Mach number, compression ratio and others) but also on the details of the electromagnetic field distribution in the shock front (in particular, shock width), especially in the case of the well-structured supercritical high-Mach number shock.

While it is clear that main energization is due to the ion interaction with the quasistationary electric and magnetic field, the role of the possible additional substructure (phasestanding waves and precursor) and time-dependent fields (coherent waves and turbulence) is apparently smoothing and adjusting the ion distribution (for example, filling

the gap in the foot near the ramp similar to what is seen in Figure 9) to provide stability and stationarity at the timescale of the order of ion gyroperiod. It should be noted that this role is not completely understood and still awaits proper theoretical description.

Additional features that could possibly affect the ion distribution, leading probably to additional gyrophase mixing and smoother distributions (including additional isotropization), and that should be included in a more complete theory and future three-dimensional simulations, are the global shock nonstationarity (which may be different in one-dimensional and three-dimensional case) and deviations of one-dimensionality. There are firm indications that the shock surface is rippled (although the typical scale and amplitude of rippling are not known so far), which would result in the mixing of ions coming from places with different conditions. This issue should be addressed also in observations, where actually such mixture is measured. Comparison with numerical simulations requires numerical modeling of the mode of operation of spacecraft devices.

Finally, one of the most direct tasks remains derivation of the expression for the foot width within the framework of the one-dimensional stationary shock model with nonspecular reflection taken into account. The corresponding expression should contain as few as possible shock parameters and reflect the dependence of the ion reflection upon the magnetic compression and β_i. Such formula is necessary for making shock width determination in the single-spacecraft measurements more reliable and precise.

Acknowledgements

This research was supported by grant 94-00047 from the United States-Israel Binational Science Foundation (BSF), Jerusalem, Israel.

References

Balikhin, M.A. and Wilkinson, W.P.: 1996, 'Ion heating within the ramp of quasi-perpendicular subcritical collisionless shocks', *Geophys. Res. Lett.*, **23**, 1063-1066.

Blandford, R. and Eichler, D.: 1987, 'Particle acceleration at astrophysical shocks: A theory of cosmic ray origin', *Phys. Rep.*, **154**, 1-75.

Brinca, A.L., Borda de Água, L. and Winske, D.: 1993, 'On the stability of nongyrotropic ion populations: A first (analytical and simulation) assessment', *J. Geophys. Res.*, **98**, 7549-7560.

Burgess, D.,Wilkinson, W.P. and Schwartz, S.J.: 1989, 'Ion distribution and thermalization at perpendicular and quasi-perpendicular supercritical collisionless shocks', *J. Geophys. Res.,* **94,** 8783-8792.

Farris, M.H., Russell, C.T. and Thomsen, M.F.: 1993, 'Magnetic structure of the low beta, quasi-perpendicular shock', *J. Geophys. Res.*, **98**, 15,285-15,294.

Forslund, D.W., Quest, K.B., Brackbill, J.U. and Lee, K.: 1984, 'Collisionless dissipation in quasi-perpendicular shocks', *J. Geophys. Res.*, **89**, 2142-2150.

Fuselier, S.A. and Schmidt, W.K.H.: 1994, 'H^+ and He^{2+} heating at the Earth's bow shock', *J. Geophys. Res.*, **99**, 11,539-11,546.

Galeev, A.A., Krasnoselskikh, V.V. and Lobzin, V.V.: 1988, 'Fine structure of the front of a quasiperpendicular supercritical shock wave', *Sov. J. Plasma Phys.*, **14**, 697-702.

Gedalin, M.: 1996a, 'Ion reflection at the shock front revisited', *J. Geophys. Res.*, **101**, 4871-4878.

Gedalin, M.: 1996b, 'Noncoplanar magnetic field in the collisionless shock front', *J. Geophys. Res.*, **101**, 11,153-11,156.

Gedalin, M.: 1996c, 'Transmitted ions and ion heating in nearly-perpendicular low-Mach number shocks', *J. Geophys. Res.,* **101**, 15,569-15,578.

Gedalin, M.: 1996d, 'Particles at quasiperpendicular collisionless shocks: Dependence on the shock scale', Multiscale Processes in Space Plasmas, in *Physics of Space Plasmas (1995), Number 14,* T. Chang and J.R. Jasperse, eds. (MIT Center for Theoretical Geo/Cosmo Plasma Physics, Cambridge, MA, 1996) (to appear).

Gedalin, M., Balikhin, M. and Krasnosselskikh, V.: 1995, Electron heating in quasiperpendicular shocks', *Adv. Space Res.*, **15**(8/9), 225-233.

Gedalin, M. and Zilbersher, D.: 1995, 'Non-diagonal ion pressure in nearly-perpendicular collisionless shocks', *Geophys. Res. Lett.*, **22**, 3279-3282.

Giacalone, J., Jokipii, J.R. and Kóta, J.: 1994, 'Ion injection and acceleration at quasi-perpendicular shocks', *J. Geophys. Res.*, **99**, 19,351-19,358.

Goodrich, C.C.: 1985, 'Numerical simulations of quasi-perpendicular collisionless shocks', in *Collisionless Shocks in the Heliosphere: Reviews of Current Research, Geophys. Monogr. Ser.,* vol. 35, edited by R.G. Stone and B.T. Tsurutani, AGU, Washington, D. C., pp.153-158 .

Goodrich, C.C. and Scudder, J.D.: 1984, 'The adiabatic energy change of plasma electrons and the frame dependence of the cross shock potential at collisionless magnetosonic shock waves', *J. Geophys. Res.*, **89**, 6654-6662.

Gosling, J.T., and Robson, A.E.: 1985, 'Ion reflection, gyration, and dissipation at supercritical shocks', in *Collisionless Shocks in the Heliosphere: Reviews of Current Research, Geophys. Monogr. Ser.,* **vol. 35**, edited by R.G. Stone and B.T. Tsurutani, AGU, Washington, D. C., p.141-152.

Gosling, J.T. and Thomsen, M.F.: 1985, 'Specularly reflected ions, shock foot thicknesses, and shock velocity determinations in space,, *J. Geophys. Res.,* **90,** 9893-9896.

Gosling, J.T., Winske, D. and Thomsen, M.F.: 1988, 'Noncoplanar magnetic fields at collisionless shocks: A test of a new approach', *J. Geophys. Res.*, **93**, 2735-2740.

Greenstadt, E.W.: 1985, 'Oblique, parallel, and quasi-parallel morphology of collisionless shocks', in *Collisionless Shocks in the Heliosphere: Reviews of Current Research, Geophys. Monogr. Ser.,* **vol. 35**, edited by R.G. Stone and B.T. Tsurutani, AGU, Washington, D. C., pp. 169-184.

Gurgiolo, C., Parks, G.K., Mauk, B.H., Lin, C.S., Anderson, K.A., Lin, R.P. and Reme, H.: 1981, 'Non-$\mathbf{E} \times \mathbf{B}$ ordered ion beams upstream of the Earth's bow shock', *J. Geophys. Res.*, **86**, 4415-4424.

Jokipii, J.R., Kóta, J. and Giacalone, J.: 1993, ' Perpendicular transport in 1- and 2-dimensional shock simulations', *Geophys. Res. Lett.*, **20**, 1759-1762.

Jones, F.C. and Ellison, D.C.: 1987, 'Noncoplanar magnetic fields, shock potentials, and ion deflection', *J. Geophys. Res.*, **92**, 11,205-11,207.

Jones, F.C. and Ellison, D.C.: 1991, 'The plasma physics of shock acceleration', *Space Sci. Rev.*, **58**, 259-346.

Kennel, C.F., Edmiston, J.P. and Hada, T.: 1985, 'A quarter century of collisionless shock research', in *Collisionless Shocks in the Heliosphere: A Tutorial Review, Geophys. Monogr. Ser.,* **vol. 34**, edited by R.G. Stone and B.T. Tsurutani, AGU, Washington, D. C., pp.1-36.

Lee, L.C., Wu, C.S. and Hu, X.W.: 1986, 'Increase of ion kinetic temperature across a collisionless shock, 1, A new mechanism', *Geophys. Res. Lett.*, **13**, 209-212.

Lee, L.C., Mandt, M.E. and Hu, X.W.: 1987, 'Increase of ion kinetic temperature across a collisionless shock, 2, A simulation study', *J. Geophys. Res.*, **92**, 13,438-13,446.

Leroy, M.M.: 1983, 'Structure of perpendicular shocks in collisionless plasma', *Phys. Fluids*, **26**, 2742-2753.

Leroy, M.M., Winske, D., Goodrich, C.C., Wu, C.S. and Papadopoulos, K.: 1982, 'The structure of perpendicular bow shocks', *J. Geophys. Res.*, **87**, 5081-5094.

Livesey, W.A., Russell, C.T. and Kennel, C.F.: 1984, 'A comparison of specularly reflected gyrating ion orbits with observed shock foot thicknesses', *J. Geophys. Res.*, **89**, 6824-6828.

Li Xinlin, Lewis, H.R., LaBelle, J., Phan, T.-D. and Treumann, R.A.: 1995, 'Characteristics of the ion pressure tensor in the earth's magnetosheath', *Geophys. Res. Lett.*, **22**, 667-670.

McKean, M.E., Omidi, N. and Krauss-Varban, D.: 1995, 'Wave and ion evolution downstream of quasi-perpendicular bow shocks', *J. Geophys. Res.*, **100**, 3427-3437.

Mellott, M.M. and Greenstadt, E.W.: 1984, 'The structure of oblique subcritical bow shocks: ISEE 1 and 2 observations', *J. Geophys. Res.*, **89**, 2151-2161.

Mellott, M.M. and Livesey, W.A.: 1987, 'Shock overshoots revisited', *J. Geophys. Res.*, **92**, 13,661-13,665.

Newbury, J.A. and Russell, C.T.: 1996, 'Observations of a very thin collisionless shock', *Geophys. Res. Lett.*, **23**, 781-784.

Paschmann, G., Sckopke, N., Bame, S.J. and Gosling, J.T.: 1982, 'Observations of gyrating ions in the foot of the nearly perpendicular bow shock', *Geophys. Res. Lett.*, **9**, 881-884.

Paschmann, G., Loidl, H., Obermayer, P., Ertl, M., Laborens, R., Sckopke, N., Baumjohann, W., Carlson, C.W. and Curtis, D.W.: 1985, 'The plasma instrument for AMPTE/IRM', *IEEE Trans. Geosci. Remote Sens.*, **GE-23**, 262-266.

Quest, K.: 19898, 'Theory and simulation of collisionless parallel shocks', *J. Geophys. Res.*, **93**, 9649-9680.

Russell, C.T., Hoppe, M.M. and Livesey, W.A.: 1982a, 'Overshoots in planetary bow shocks', *Nature*, **296**, 45-48.

Russell, C.T., Hoppe, M.M., Livesey, W.A., Gosling, J.T. and Bame, S.J.: 1982b, 'ISEE-1 and -2 observations of laminar bow shocks: Velocity and thickness', *Geophys. Res. Lett.*, **9**, 1171-1174.

Scholer, M. and Fujimoto, M.: 1993, 'Low-Mach number quasi-parallel shocks: Upstream waves', *J. Geophys. Res.*, **98**, 15,275-15,283.

Schwartz, S.J., Thomsen, M.F. and Gosling, J.T.: 1983, 'Ions upstream of the Earth's bow shock: A theoretical comparison of alternative source population', *J. Geophys. Res.*, **88**, 2039-2047.

Sckopke, N., Paschmann, G., Bame, S.J., Gosling, J.T. and Russell, C.T.: 1983, 'Evolution of ion distributions across the nearly perpendicular bow shock: Specularly and nonspecularly reflected-gyrating ions', *J. Geophys. Res.*, **88**, 6121-6136.

Sckopke, N., Paschmann, G., Brinca, A.L., Carlson, C.W. and Lühr, H.: 1990, 'Ion thermalisation in quasi-perpendicular shocks involving reflected ions', *J. Geophys. Res.*, **95**, 6337-6352.

Scudder, J.D., Mangeney, A., Lacombe, C., Harvey, C.C., Aggson, T.L., Anderson, R.R., Gosling, J.T., Paschmann, G. and Russell, C.T.: 1986a, 'The resolved layer of a collisionless, high β, supercritical, quasi-perpendicular shock wave, 1, Rankine-Hugoniot geometry, currents, and stationarity', *J. Geophys. Res.*, **91**, 11,019-11,052.

Scudder, J.D., Mangeney, A., Lacombe, C. and Harvey, C.C.: 1986b, 'The resolved layer of a collisionless, high β, supercritical, quasi-perpendicular shock wave, 2, Dissipative fluid hydrodynamics', *J. Geophys. Res.*, **91**, 11,053-11,073.

Thomsen, M.F., Gosling, J.T., Bame, S.J. and Mellott, M.M.: 1985, 'Ion and electron heating at collisionless shocks near the critical Mach number', *J. Geophys. Res.*, **90**, 137-148.

Wilkinson, W.P.: 1991, 'Ion kinetic processes and thermalization at quasi-perpendicular low-Mach number shocks', *J. Geophys. Res.*, **96**, 17,675-17,688.

Wilkinson, W.P. and Schwartz, S.J.: 1990, 'Parametric dependence of the density of specularly reflected ions at quasiperpendicular collisionless shocks', *Planet. Space Sci.*, **38**, 419-435.

Wilkinson, W.P., Pardaens, A.K., Schwartz, S.J., Burgess, D., Lühr, H., Kessel, R.L., Dunlop, M. and Farrugia, C.J.: 1993, 'Nonthermal ions and associated magnetic field behavior at a quasi-parallel Earth's bow shock', *J. Geophys. Res.*, **98**, 3889-3905.

Woods, L.C.: 1969, 'On the structure of collisionless magnetoplasma shock waves at supercritical Alfven Mach numbers', *J. Plasma Phys.*, **3**, 435-447.

Woods, L.C.: 1971, 'On double structured, perpendicular, magneto-plasma shock waves', *J. Plasma Phys.*, **13**, 281.

Wygant, J.R., Bensadoun, M. and Mozer, F.C.: 1987, ' Electric field measurements at subcritical, oblique bow shock crossings', *J. Geophys. Res.*, **92**, 11,109-11,121.

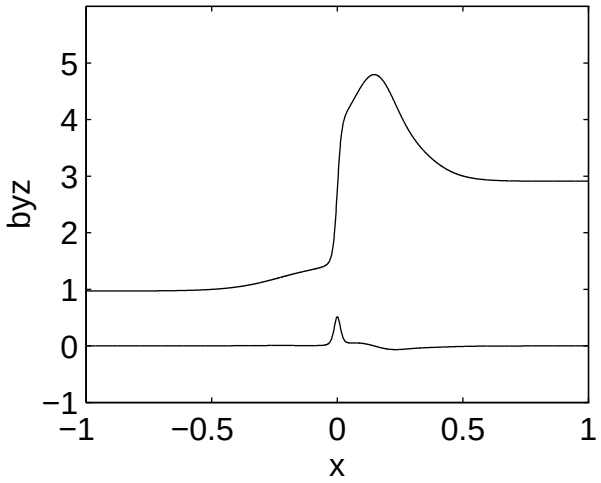

Figure 1. (a) Magnetic field profile of a high-Mach number supercritical quasiperpendicular collisionless shock (from Russell *et al.*, 1982a, Fid. 2a), and (b) well-accepted theoretical approximation for this profile (qualitatively).

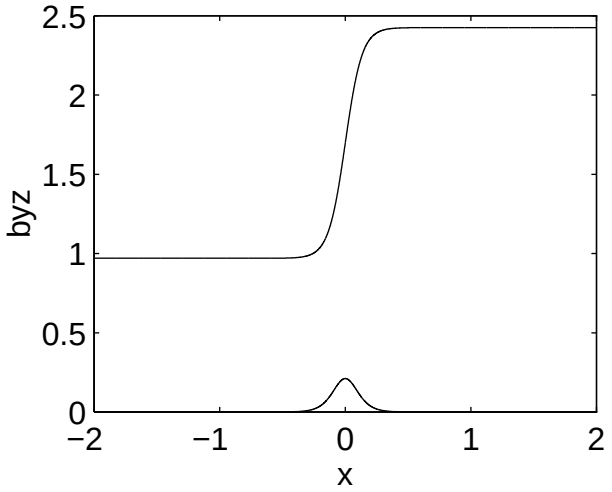

Figure 2. (a) Magnetic field profile of a low-Mach number shock (from Russell *et al.*, 1982a, Fig. 2a), and (b) the corresponding theoretical approximation (qualitatively).

Figure 3. A sequence of ion distributions measured at a high-Mach number shock (from Sckopke *et al.*, 1983, Fig. 2).

Figure 4. Velocity space distributions of specular reflected ions for oblique shock geometry and two opposing field orientations (from Sckopke *et al.*, 1983, Fig. 1).

Figure 5. Ion distribution function for the case of Figure 3 (from Sckopke *et al.*, 1983, Fig. 15).

Figure 6. A sequence of ion distributions measured at a low-Mach number shock (from Sckopke *et al.*, 1983, Fig. 10).

Figure 7. Ion distributions measured at a very low-Mach number shock (from Thomsen *et al.*, 1985, Fig. 12).

Figure 8. Two-dimensional cuts of the three-dimensional ion distribution measured by AMPTE-IRM at a low-Mach number shock (from Sckopke *et al.*, 1990, Fig. 3).

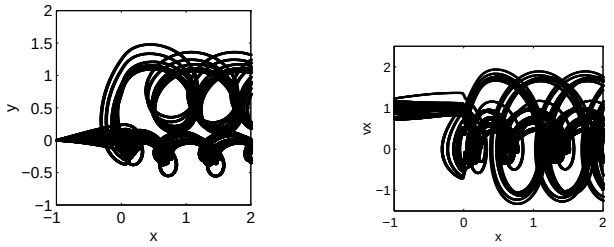

Figure 9. Trajectories of 25 ions in the model high-Mach number shock front.

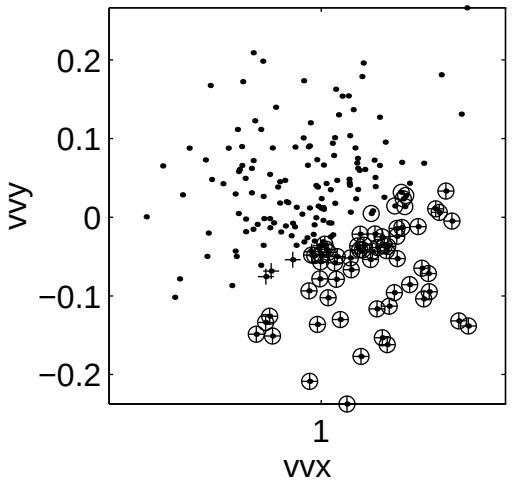

Figure 10. Part of the incident ion distribution which is reflected (from Gedalin, 1996a, Fig. 5a): Maxwellian distribution of incident ions (all the symbols together), ions which are found to be reflected analytically (crosses) and numerically (open circles).

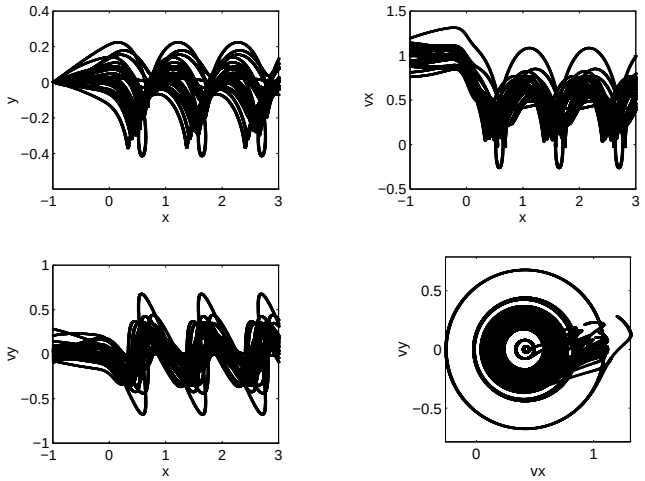

Figure 11. Trajectories of 25 ions in the model low-Mach number shock front.

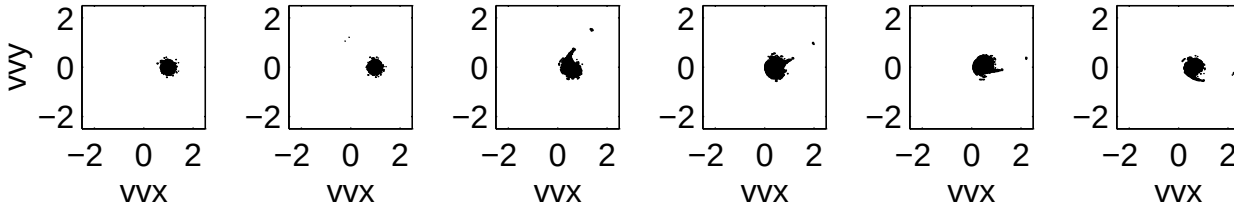

Figure 12. Ion distributions in the very low-Mach number shock in several places (from Gedalin, 1996c).

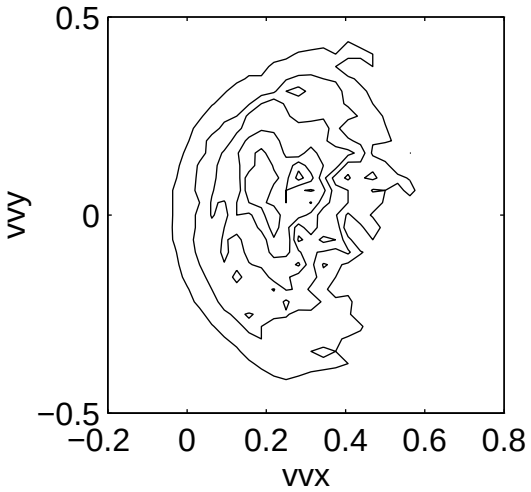

Figure 13. Typical downstream ion distribution in the low-Mach number shock (from Gedalin, 1996c.)